

Melting and transverse depinning of driven vortex lattices in the periodic pinning of Josephson junction arrays

Verónica I. Marconi and Daniel Domínguez

Centro Atómico Bariloche, 8400 San Carlos de Bariloche, Río Negro, Argentina

We study the non-equilibrium dynamical regimes of a moving vortex lattice in the periodic pinning of a Josephson junction array (JJA) for *finite temperatures* in the case of a fractional or submatching field. We obtain a phase diagram for the current driven JJA as a function of the driving current I and temperature T . We find that when the vortex lattice is driven by a current, the depinning transition at $T_p(I)$ and the melting transition at $T_M(I)$ become separated even for a field for which they coincide in equilibrium. We also distinguish between the depinning of the vortex lattice in the direction of the current drive, and the *transverse depinning* in the direction perpendicular to the drive. The transverse depinning corresponds to the onset of transverse resistance in a moving vortex lattice at a given temperature T_{tr} . For driving currents above the critical current we find that the moving vortex lattice has first a transverse depinning transition at low T , and later a melting transition at a higher temperature, $T_M > T_{tr}$.

PACS numbers: 74.50+r, 74.60.Ge, 74.60.Ec

I. INTRODUCTION

The behavior of superconducting vortices in the presence of periodic pinning shows very rich static and dynamic phenomena.^{1–24} The competition between the repulsive vortex-vortex interaction and the attractive periodic pinning potential results in novel vortex structures at low temperatures.^{3,8–10,16,17} The equilibrium phase transitions of these vortex structures and their various dynamical regimes when driven out of equilibrium are of great interest both experimentally^{1–9,12} and theoretically.^{3,10–24} Several techniques have been developed to fabricate in superconducting samples an artificial periodic pinning structure: thickness modulated superconducting films,¹ superconducting wire networks,² Josephson junction arrays,^{3–5} magnetic dot arrays,⁶ sub-micron hole lattices,^{7,8} and pinning induced by Bitter decoration.⁹ The ground states of these systems can be either commensurate or incommensurate vortex structures depending on the vortex density (i.e the magnetic field). In the commensurate case, a “matching” field is defined when the number of vortices N_v is an integer multiple of the number of pinning sites N_p : $N_v = nN_p$. A “submatching” or “fractional” field is defined when N_v is a rational multiple of N_p : $N_v = fN_p$ with $f = p/q$. One of the main properties of periodic pinning is that there are enhanced critical currents and resistance minima both for fractional and for matching magnetic fields, for which the vortex lattice is strongly pinned.

In the case of Josephson junction arrays³ (JJA) the discrete lattice structure of Josephson junctions induces an effective periodic pinning potential (the so-called “egg-carton” potential) which at low temperatures confines the vortices at the centers of the unit cells of the network.⁴ There are strong commensurability effects for submatching fields $f = p/q$, for which the vortices arrange in an ordered $q \times q$ superlattice that is commensurate with the underlying array of junctions. The transition temperature $T_c(f)$ and the critical current $I_c(f)$

have maxima for rational $f = p/q$, which have been observed experimentally.^{3,5} Moreover, as we will discuss here, the model that describes the physics of the JJA can be thought as a discrete lattice London model for thin film superconductors with periodic arrays of holes. However, this comparison can be valid only for low submatching fields since it can not describe the effects of interstitial vortices.

The equilibrium phase transitions at finite temperatures of two dimensional systems with periodic pinning have been studied in the past.^{11–15} It is possible to have a depinning phase transition of the commensurate ground states at a temperature T_p and a melting transition of the vortex lattice at a temperature T_M .^{11–15} Franz and Teitel¹⁴ have studied this problem for the case of submatching fields. For $0 < T < T_p$ there is a pinned phase in which the vortex lattice (VL) is pinned commensurably to the periodic potential and has long-range order. For $T_p < T < T_M$ there is a floating VL which is depinned and has quasi-long-range order. For high submatching fields ($f \gtrsim 1/30$) both transitions coincide, $T_p = T_M$, while for low submatching fields ($f \lesssim 1/30$) both transitions are different with $T_p < T_M$.^{14,15}

The non-equilibrium dynamics of driven vortex lattices interacting either with random or periodic pinning shows an interesting variety of behavior.^{18–31} Many recent studies have concentrated in the problem of the driven VL in the presence of *random* pinning.^{25–31} When there is a large driving current the effect of the pinning potential is reduced, and the nature of the fastly moving vortex structure has been under active discussion. The moving vortex phase has been proposed to be either a crystalline structure, a moving glass, a moving smectic or a moving transverse glass.^{25–27} These moving phases have been studied both experimentally²⁸ and numerically.^{29–31} Motivated by these results, the dynamical regimes of the moving VL in the presence of *periodic* pinning has also become a subject of interest.^{18–24} At zero temperature, the dynamical phases of vortices driven by an external

current with a periodic array of pinning sites has been studied in very detail by F. Nori and coworkers.^{18,19} A complex variety of regimes has been found, particularly for $N_v > N_p$ where the motion of interstitial vortices leads to several interesting dynamical phases.

In this paper we study the dynamical regimes of a moving VL in the periodic pinning of a Josephson junction array (JJA) for *finite temperatures* in the case of a *sub-matching* field ($f = 1/25$). We obtain a phase diagram as a function of the driving current I and temperature T , which is shown in Fig. 1. We find that when the VL is driven by a low current, the depinning and melting transitions can become separated even for a field for which they coincide in equilibrium. Moreover, we can distinguish between the depinning of the VL in the direction of the current drive, and the *transverse depinning* in the direction perpendicular to the drive. This later case corresponds to the vanishing of the transverse critical current in a moving VL at a given temperature T_{tr} , or equivalently, to the vanishing of the transverse superconducting coherence. We obtain three distinct regimes at low temperatures: (i) *Pinned vortex lattice*: for $0 < T < T_p(I)$ there is an ordered VL which has crystalline long-range order, superconducting coherence (i.e., a finite helicity modulus) and zero resistance both in the longitudinal and transverse directions. (ii) *Transversely pinned vortex lattice*: for $T_p(I) < T < T_{tr}(I)$ there is a moving VL which has anisotropic Bragg peaks, quasi-long range order, transverse superconducting coherence and zero transverse resistivity. There is a finite transverse critical current. This regime also has strong orientational pinning effects²⁴ in the $[1,0]$ and $[0,1]$ lattice directions. (iii) *Floating vortex lattice*: for $T_{tr}(I) < T < T_M(I)$ there is a moving VL which is unpinned in both directions and it has quasi-long range crystalline order with a strong anisotropy. Some of the results we discuss here were reported by us previously in a shorter and less detailed version.²⁰ After our work in Ref. 20, further studies of thermal effects in a moving vortex lattice with a periodic pinning array have been reported for $N_v = N_p$ ²² and for $N_v > N_p$.^{21,23} Some of these results are similar to ours.

The remainder of our paper is organized as follows. In Sec. II we introduce the theoretical model used for the dynamics of the JJA. We also discuss how this model can be mapped to a superconducting film with a periodic array of holes. In Sec. III we discuss the melting transition near equilibrium when the JJA is driven by a very small current. In Sec. IV we present our results for the transport properties, analyzing the temperature dependence of the current-voltage curves and the onset of resistivity at T_p for different currents. In Sec. V we present our results for the transverse depinning transitions at different temperatures and driving currents. We study the transverse current-voltage characteristics both at $T = 0$ and at finite T . We define the transverse depinning temperature T_{tr} from the behavior of the transverse resistivity. In Sec. VI we present in detail our results for the different dynamical regimes. For various fixed

driving currents, we analyze the behavior of structure factor, longitudinal and transverse resistance and helicity modulus through the different regimes as a function of temperature. These results constitute the central core of this paper, from which the phase diagram of Fig. 1 was obtained. In Sec. VII we discuss the orientational pinning effects, which are observed when the direction of the driving current is rotated with respect to the JJA square lattice. Finally in Sec. VIII we present our discussion and conclusions. We also add an Appendix at the end, where we provide a detailed definition of the adequate periodic boundary conditions for a JJA with an external magnetic field and an external driving current, as well as the algorithm used for the numerical simulation.

II. MODEL AND DYNAMICS

A. RSJ dynamics

We consider a square Josephson junction array with $L \times L$ superconducting nodes. The nodes are in the lattice sites $\mathbf{n} = (n_x, n_y)$ and their superconducting phases are $\theta(\mathbf{n})$. We study the dynamics of JJA using the resistively shunted junction (RSJ) model for the junctions of the square network.^{32–35,?,38} In this case, the current flowing in the junction between two superconducting nodes in the JJA is modeled as the sum of the Josephson supercurrent and the normal current:

$$I_\mu(\mathbf{n}) = I_0 \sin \theta_\mu(\mathbf{n}) + \frac{\hbar}{2eR_N} \frac{d\theta_\mu(\mathbf{n})}{dt} + \eta_\mu(\mathbf{n}, t) \quad (1)$$

where I_0 is the critical current of the junction between the sites \mathbf{n} and $\mathbf{n} + \mu$, ($\mu = \hat{x}, \hat{y}$), R_N is the normal state resistance and

$$\theta_\mu(\mathbf{n}) = \theta(\mathbf{n} + \mu) - \theta(\mathbf{n}) - A_\mu(\mathbf{n}) = \Delta_\mu \theta(\mathbf{n}) - A_\mu(\mathbf{n}) \quad (2)$$

is the gauge invariant phase difference with

$$A_\mu(\mathbf{n}) = \frac{2\pi}{\Phi_0} \int_{\mathbf{n}\mathbf{a}}^{(\mathbf{n}+\mu)\mathbf{a}} \mathbf{A} \cdot d\mathbf{l}. \quad (3)$$

The thermal noise fluctuations η_μ have correlations

$$\langle \eta_\mu(\mathbf{n}, t) \eta_{\mu'}(\mathbf{n}', t') \rangle = \frac{2kT}{R_N} \delta_{\mu, \mu'} \delta_{\mathbf{n}, \mathbf{n}'} \delta(t - t') \quad (4)$$

In the presence of an external magnetic field H we have

$$\begin{aligned} \Delta_\mu \times A_\mu(\mathbf{n}) &= A_x(\mathbf{n}) - A_x(\mathbf{n} + \mathbf{y}) + A_y(\mathbf{n} + \mathbf{x}) - A_y(\mathbf{n}) \\ &= 2\pi f, \end{aligned} \quad (5)$$

$f = Ha^2/\Phi_0$ and a is the array lattice spacing. We take periodic boundary conditions (p.b.c) in both directions in the presence of an external current $\mathbf{I} = I\hat{y}$ in arrays

with $L \times L$ junctions.³¹ (See the Appendix). The vector potential is taken as

$$A_\mu(\mathbf{n}, t) = A_\mu^0(\mathbf{n}) - \alpha_\mu(t) \quad (6)$$

where in the Landau gauge $A_x^0(\mathbf{n}) = -2\pi f n_y$, $A_y^0(\mathbf{n}) = 0$ and $\alpha_\mu(t)$ allows for total voltage fluctuations under periodic boundary conditions. In this gauge the p.b.c. for the phases are:^{20,31}

$$\begin{aligned} \theta(n_x + L, n_y) &= \theta(n_x, n_y) \\ \theta(n_x, n_y + L) &= \theta(n_x, n_y) - 2\pi f L n_x. \end{aligned} \quad (7)$$

We also consider local conservation of current,

$$\Delta_\mu \cdot I_\mu(\mathbf{n}) = \sum_\mu I_\mu(\mathbf{n}) - I_\mu(\mathbf{n} - \mu) = 0. \quad (8)$$

After Eqs. (1,8) we obtain the following equations for the phases,^{20,31}

$$\frac{\hbar}{2eR_N} \Delta_\mu^2 \frac{d\theta(\mathbf{n})}{dt} = -\Delta_\mu \cdot [S_\mu(\mathbf{n}) + \eta_\mu(\mathbf{n}, t)] \quad (9)$$

where

$$S_\mu(\mathbf{n}) = I_0 \sin[\Delta_\mu \theta(\mathbf{n}) - A_\mu^0(\mathbf{n}) - \alpha_\mu], \quad (10)$$

and the discrete Laplacian is

$$\Delta_\mu^2 f(\mathbf{n}) = f(\mathbf{n} + \hat{\mathbf{x}}) + f(\mathbf{n} - \hat{\mathbf{x}}) + f(\mathbf{n} + \hat{\mathbf{y}}) + f(\mathbf{n} - \hat{\mathbf{y}}) - 4f(\mathbf{n}). \quad (11)$$

The Laplacian can be inverted with the square lattice Green's function $G_{\mathbf{n}, \mathbf{n}'}$:

$$\Delta_\mu^2 G_{\mathbf{n}, \mathbf{n}'} = \delta_{\mathbf{n}, \mathbf{n}'}. \quad (12)$$

Since we take periodic boundary conditions (see Appendix), the total current has to be fixed by:

$$I_x = \frac{1}{L^2} \left[\sum_{\mathbf{n}} I_0 \sin \theta_x(\mathbf{n}) + \eta_x(\mathbf{n}, t) \right] + \frac{\hbar}{2eR_N} \frac{d\alpha_x}{dt}, \quad (13)$$

$$I_y = \frac{1}{L^2} \left[\sum_{\mathbf{n}} I_0 \sin \theta_y(\mathbf{n}) + \eta_y(\mathbf{n}, t) \right] + \frac{\hbar}{2eR_N} \frac{d\alpha_y}{dt},$$

These equations determine the dynamics of $\alpha_\mu(t)$.³¹ For this case we take $I_x = 0$ and $I_y = I$. After Eqs. (9,12,13) we obtain the following set of dynamical equations,^{20,31}

$$\frac{d\theta(\mathbf{n})}{dt} = - \sum_{\mathbf{n}'} G_{\mathbf{n}, \mathbf{n}'} \Delta_\mu \cdot [S_\mu(\mathbf{n}') + \eta_\mu(\mathbf{n}', t)], \quad (14)$$

$$\frac{d\alpha_\mu}{dt} = I_\mu - \frac{1}{L^2} \sum_{\mathbf{n}} S_\mu(\mathbf{n}) + \eta_\mu(\mathbf{n}, t), \quad (15)$$

where we have normalized currents by I_0 , time by $\tau_J = 2eR_N I_0 / \hbar$, and temperature by $I_0 \Phi_0 / 2\pi k_B$.

B. Comparison with thin film with a periodic array of holes

Let us consider a superconducting thin film with a square array of holes, which act as pinning sites for vortices. There are $N_p = L^2$ pinning sites separated by a distance a . The current density in the superconducting film is given by the sum of the supercurrent and the normal current:

$$\begin{aligned} \mathbf{J} &= \mathbf{J}_S + \mathbf{J}_N \\ \mathbf{J} &= \frac{ie\hbar}{m^*} [\Psi^* \mathbf{D} \Psi - (\mathbf{D} \Psi)^* \Psi] + \frac{\sigma \Phi_0}{2\pi c} \frac{\partial}{\partial t} \left(\nabla \theta - \frac{2\pi}{\Phi_0} \mathbf{A} \right) \end{aligned} \quad (16)$$

with $\mathbf{D} = \nabla + i\frac{2\pi}{\Phi_0} \mathbf{A}$, $\Psi(\mathbf{r}) = |\Psi(\mathbf{r})| \exp[i\theta(\mathbf{r})]$ the superconducting order parameter and σ the normal state conductivity. These equations are valid everywhere in the film except in the hole regions. If the number of vortices $N_v = BL^2 a^2 / \Phi_0$ is much smaller than the number of pinning sites N_p , all vortices will be centered in the holes in equilibrium. In this case we can assume that $|\Psi(\mathbf{n})| \approx |\Psi_0|$ is homogeneous in the superconducting film. Therefore the dynamics is given by the superconducting phase $\theta(\mathbf{r})$, corresponding to a London model in a sample with holes. After considering current conservation $\nabla \cdot \mathbf{J} = 0$, we obtain the London dynamical equations for the phases in this multiply connected geometry. Since $N_v \ll N_p$, we make the approximation of solving the equations in a discrete grid of spacing a . This means that we take as the relevant dynamical variables the phases $\theta(\mathbf{r}_\mathbf{n})$ defined in the sites which are dual to the pinning sites. They represent the average superconducting phase in each superconducting square defined by four pinning sites. Therefore, we take the discretization $\mathbf{r}_\mathbf{n} = (n_x a, n_y a) = \mathbf{a}\mathbf{n}$. [Pinning sites at centered at positions $\mathbf{r}_\mathbf{p} = (n_x + 1/2, n_y + 1/2)a$]. The derivatives in the supercurrent are discretized in a gauge-invariant way as

$$D_\mu \Psi(\mathbf{r}) \rightarrow \frac{1}{a} \left[\Psi(\mathbf{n} + \mu) - e^{-i2\pi A_\mu(\mathbf{n}) / \Phi_0} \Psi(\mathbf{n}) \right]. \quad (17)$$

After doing this, we obtain an equation analogous to (1). Now $I_\mu(\mathbf{n})$ has to be interpreted as current density normalized by $J_0 = 2e\hbar |\Psi_0|^2 / ma = \Phi_0 / (8\pi^2 \lambda^2 a)$, time normalized by $\tau = c / (4\pi \sigma \lambda^2)$, and the fraction of vortices is $f = N_v / N_p = Ba^2 / \Phi_0$. This leads to a set of dynamical equations of the same form as Eqs.(14,15). Therefore, we expect that for $f \ll 1$ the model for a JJA also gives a good representation of the physics of a superconducting film with a square array of holes (meaning that effects of interstitial vortices are neglected for $N_v \ll N_p$). In other words, we expect that for a low density of vortices the specific shape of the periodic pinning potential (being either an egg-carton or an array of holes) will not be physically relevant.

C. Quantities calculated and simulation parameters

The Langevin dynamical equations (14,15) are solved with a second order Runge-Kutta-Helfand-Greenside algorithm with time step $\Delta t = 0.1\tau_J$. The discrete periodic Laplacian is inverted with a fast Fourier + tridiagonalization algorithm as in Ref. 35. (See also the Appendix).

We calculate the following physical quantities:

(i) *Transverse superconducting coherence*: We obtain the helicity modulus Υ_x in the direction transverse to the current as

$$\Upsilon_x = \frac{1}{L^2} \left\langle \sum_{\mathbf{n}} \cos \theta_x(\mathbf{n}) \right\rangle - \frac{1}{TL^4} \left\{ \left\langle \left[\sum_{\mathbf{n}} \sin \theta_x(\mathbf{n}) \right]^2 \right\rangle - \left\langle \left[\sum_{\mathbf{n}} \sin \theta_x(\mathbf{n}) \right] \right\rangle^2 \right\}$$

Whenever we calculate the helicity modulus along x , we enforce strict periodicity in θ by fixing $\alpha_x(t) = 0$. (See Appendix).

(ii) *Transport*: We calculate the transport response of the JJA from the time average of the total voltage as

$$\begin{aligned} V_x &= \langle v_x(t) \rangle = \langle d\alpha_x(t)/dt \rangle \\ V_y &= \langle v_y(t) \rangle = \langle d\alpha_y(t)/dt \rangle \end{aligned} \quad (18)$$

with voltages normalized by $R_N I_0$.

(iii) *Vortex structure*: We obtain the vorticity at the plaquette $\tilde{\mathbf{n}} = (n_x + 1/2, n_y + 1/2)$ (associated to the site \mathbf{n}) as³⁹

$$b(\tilde{\mathbf{n}}) = -\Delta_\mu \times \text{nint}[\theta_\mu(\mathbf{n})/2\pi] \quad (19)$$

with $\text{nint}[x]$ the nearest integer of x . We calculate the average vortex structure factor as

$$S(\mathbf{k}) = \left\langle \left| \frac{1}{L^2} \sum_{\tilde{\mathbf{n}}} b(\tilde{\mathbf{n}}) \exp(i\mathbf{k} \cdot \tilde{\mathbf{n}}) \right|^2 \right\rangle. \quad (20)$$

III. TRANSITION NEAR EQUILIBRIUM

We study JJA with a low magnetic field corresponding to $f = 1/25$, for different system sizes of $L \times L$ junctions, with $L = 50, 100, 150$. Most of the results are for $L = 100$, except when it is explicitly specified, and for $N_t = 10^5$ iterations after a transient of $N_t/2$ iterations.

The ground state vortex configuration for $f = 1/25$ is a tilted square-like vortex lattice (VL),⁴⁰ see Fig.2(a). We find that this state is stable for low currents and low temperatures (in fact, the structure of Fig.2(a) corresponds to $I = 0.01$ and $T = 0.01$). The lattice is oriented in the $[4a, 3a]$ direction and commensurated with the underlying periodic pinning potential of the square JJA. The

structure factor $S(\mathbf{k})$ has the corresponding Bragg peaks at wavevectors \mathbf{G} in the reciprocal space, as can be seen in Fig.1(b). When the temperature is increased, the VL tends to disorder and above the melting temperature T_M a random vortex array with a liquid-like structure factor is obtained, Figs. 2(c) and 2(d).

We find a single equilibrium phase transition ($I = 0$) at $T_M \approx 0.050 \pm 0.003$, which is in agreement with the melting temperature obtained by Franz and Teitel¹⁴ and Hattel and Wheatley¹⁵ for $f \gtrsim 1/30$.

We now apply a very low current, $I = 0.01$, in order to study the near-equilibrium transport response simultaneously with other quantities like structure factor and helicity modulus. We find a phase transition at a temperature $T_M(I) \approx 0.046 \pm 0.001$, which is slightly lower than the equilibrium transition. In Fig.3(a) we see that there is a large jump in the resistance $R = V/I$ at T_c , in good agreement with the first-order nature of the equilibrium transition.¹⁴ The onset of resistivity is a signature of a depinning transition in the direction of the drive. This occurs simultaneously with a melting of the vortex lattice, corresponding to the vanishing of Bragg peaks, as shown in Fig.3(b) for the two first reciprocal lattice vectors $\mathbf{G}_1 = \frac{2\pi}{a}(-4/25, -3/25)$ and $\mathbf{G}_2 = \frac{2\pi}{a}(-3/25, 4/25)$. The size dependence of $S(\mathbf{G}, T)$ is shown in the inset of Fig.3(b). In the direction of the current drive the helicity modulus is ill-defined since total phase fluctuations are allowed. (See the Appendix). However, in the perpendicular direction to the drive the helicity modulus Υ_x can be calculated, and it is a measure of the transverse superconducting coherence. As we can see in Fig.3(c), transverse superconductivity also vanishes at $T_M(I)$. Above T_M , we find that the $\Upsilon_x(T)$ has large fluctuations around zero.

IV. TRANSPORT PROPERTIES

Let us now study the transport properties for larger currents. We calculate the current-voltage (IV) characteristics for different temperatures as well as the dc resistance $R = V/I$ as a function of temperature for finite currents.

The zero temperature IV curve has a critical current, $I_c(0) = 0.114 \pm 0.002$, see Fig.4, which corresponds to the single vortex depinning current in square JJA,⁴ with the typical square root dependence at the onset. Similar behavior has been reported for zero temperature IV curves for low values of f .^{37,38} Above $I_c(0)$ there is an almost linear increase of voltage, corresponding to a ‘‘flux flow’’ regime, where there is a fastly moving VL. The structure factor of the $T = 0$ moving VL is the same as the corresponding one of the pinned VL [Fig.2(a)]. The presence of periodic boundary conditions in our case prevents the occurrence of random or chaotic vortex motion near the critical current, as reported in early simulations with free boundary conditions.^{32,33} In what follows we will restrict

our analysis for currents $I < 0.4$, where the collective behavior of the VL is the dominant physics. (At $I \sim 1$ there is a sharp increase of voltage when all the junctions become normal, and $V \sim R_N I$ for $I \gg 1$).

The IV curves for finite temperatures are shown in Fig.5. For temperatures below T_M there is a nonlinear sharp rise in voltage which defines the apparent critical current $I_c(T)$. For example, we can obtain this $I_c(T)$ with a voltage criterion, which we choose as $V < \frac{1}{N_t \Delta t} = 10^{-4}$. In this case, we find that $I_c(T)$ decreases with T , vanishing at T_M . It is interesting to point out that all the IV curves for different temperatures have a crossing point at $I^* = 0.165$, see Fig.5(a). A crossing in the IVs has also been reported in experiments in amorphous thin films.⁴¹ For temperatures $T > T_M$ the IV curves tend to linear resistivity for low currents. This is shown in Fig.5(b) in a log-log plot of $R(I) = V/I$ vs I , where we see that $R(I)$ tends to a low current finite value for $T > T_M$, while it has a strong nonlinear decrease for $T < T_M$.

Let us now study the dc resistance $R = V/I$ as a function of temperature for a given applied current in the y -direction (Fig.6). We start with the perfectly ordered VL as an initial condition at $T = 0$ and then we slowly increase the temperature, keeping I constant. For currents below the $T = 0$ critical current, $I < I_c(0)$, the dc resistance is negligibly small at low T , and it has a steep increase at a depinning temperature $T_p(I)$, corresponding to the onset of vortex motion. The depinning temperature decreases for increasing currents, and the values of $T_p(I)$ are coincident with the apparent critical currents $I_c(T)$ obtained from the IV curves. For currents higher than $I_c(0)$, there is always a large and finite voltage for any temperature. If $I_c(0) < I < I^*$, the $R(I)$ increases slightly with T tending to a constant value for large T , while for $I > I^*$ the $R(I)$ decreases with T .

V. TRANSVERSE DEPINNING

What is its response to a small current in the transverse direction when the driven vortex lattice is moving? Is the vortex lattice still pinned in the transverse direction? Is there a transverse critical current for a moving VL? The idea of a transverse depinning current was introduced by Giamarchi and Le Doussal in Ref. 26 for moving vortex systems with random pinning at zero temperature. The possibility of such a critical current was later questioned by Balents, Marchetti and Radzihovsky,²⁷ where it was shown that this is not true for any finite temperature in *random pinning*; however a strong nonlinear increase of the transverse voltage was predicted at an “effective” transverse critical current. In the case of *periodic pinning* it is more clear that a transverse critical current will exist at $T = 0$ since it is a commensurability effect. This has been found in the $T = 0$ simulation work of Reichhardt *et al.*¹⁸ It is also possible that this transverse critical current will still be non-zero at $T \neq 0$ in *periodic pinning*.

In fact, we have found in our previous work²⁰ that there is a *thermal* transverse depinning in a *periodic* system, and we will now analyze this behavior in detail.

First, a high longitudinal current $I > I_c(0)$ is applied at zero temperature. Then, a current I_{tr} is applied in the transverse direction. In this way, a transverse current-voltage characteristics can be obtained for each I . This is shown in Fig.7(a) for $I = 0.16$. We clearly see that there is a finite transverse critical current $I_{c,tr} \approx 0.12$, which is of the order of the single vortex pinning barrier. We also show in Fig.7(a) how the longitudinal voltage V changes when the transverse current is varied. For $I_{tr} < I_{c,tr}$ the longitudinal voltage V is almost constant. At $I_{c,tr}$ there is a fast decay of V . When $I_{tr} = I$ we also have $V = V_{tr}$ as expected for a drive at a degree of $\pi/4$. Later, for $I_{tr} > I$ the vortex lattice becomes pinned in the other direction, since now the directions of “longitudinal” and “transverse” current are interchanged.

Another possible measurement is to study thermal transverse depinning. In this case, we start with a longitudinal current I , then a small transverse current is applied, $I_{tr} \ll I_{c,tr}$, and the temperature is slowly increased. In this way, we can measure a transverse resistance $R_{tr} = V_{tr}/I_{tr}$. In Fig.7(b) we plot this result for $I = 0.16$ and $I_{tr} = 0.01$. We find that for finite low temperatures R_{tr} is negligibly small within our numerical accuracy and it has a clear onset at a transverse critical temperature T_{tr} .

Let us now see how these results depend on the longitudinal current I and temperature T . We have calculated the transverse IV (Tr-IV) curves for different I and T . In Fig.8(a) we show the Tr-IV curves for $I = 0.06$ (low current regime) and in Fig.8(b) for $I = 0.16$ (high current regime). In both cases, there is a clear change of behavior in the Tr-IV curves when going through a characteristic transverse critical temperature $T_{tr}(I)$. For low temperatures there is a transverse critical current which tends to vanish when T approaches $T_{tr}(I)$ from below. In contrast, for $T > T_{tr}$ there is a linear resistivity behaviour.

The transverse resistivity $R_{tr} = V_{tr}/I_{tr}$ as a function of temperature was calculated for different longitudinal currents (Fig.9). In all cases there is an onset of transverse response at a given temperature $T_{tr}(I)$. At low currents, $I < I_c(0)$, the transverse depinning temperatures are almost constant, $T_{tr} \sim 0.02$ tending to increase slowly with I , see Fig.9(a). On the other hand, for $I > I_c(0)$ the transverse depinning temperatures increase clearly with I , see Fig.9(b).

VI. NON-EQUILIBRIUM REGIMES

We will now study the different non-equilibrium regimes of vortex driven lattices and characterize their possible dynamical transitions. The approach we will follow in this Section is to have a fixed current applied in the system and vary the temperature. In this way, we

look for the possible transitions as a function of T in a similar way as was done near equilibrium in Sec.III.

A few similar studies were done previously in related systems. In Ref. 30 the melting transition of a moving vortex lattice in the three dimensional XY model was studied in this way. In this work a first order transition was found as a function of temperature in a strongly driven vortex lattice. In Ref. 36 a current driven two dimensional JJA at zero field was studied. The possibility of a transition as a function of temperature for finite currents below the critical current was analyzed in this case.

In the following, we will separate our study in three ranges of current: (i) low currents, $I < 0.04$, (ii) intermediate currents $0.04 < I < I_c(0)$, and high currents $I > I_c(0)$.

A. Low currents

We show the results for a low current in Fig.10 for $I = 0.03$. The longitudinal dc response, V/I , is negligibly small at low T and later it has a sharp increase of two orders of magnitude: this defines the *depinning temperature*, T_p [Fig.10(a)]. At higher temperatures, $T > T_p$, the resistance is weakly T -dependent.

Below T_p the vortex lattice is pinned and its structure is similar to the ground state: a vortex lattice commensurate with the underlying square array and tilted in the $[4a, 3a]$ direction. Above T_p the vortex lattice is moving and it has an anisotropic structural order. If we analyze the structure factor in two different reciprocal lattice directions $S(G_1)$ and $S(G_2)$, we can see this clearly (Fig.10(b)). Below T_p the VL structure is isotropic and $S(G_1) = S(G_2)$. Right above T_p the height of the peaks decreases with temperature, and the structure of the depinned VL is clearly anisotropic, $S(G_1) \neq S(G_2)$. Finally, at a melting temperature T_M the peaks vanish, and the vortex lattice melts into a vortex liquid. In Fig.11 we compare the behavior of the Bragg peaks for two system sizes $L = 50, 100$. We see that the $S(G_{1,2})$ are size independent below T_p as it should be expected for a pinned phase.¹⁴ For large temperatures $T > T_M$, in the liquid phase, the value of $S(G_{1,2})$ is strongly size dependent, since it should go as L^{-2} .¹⁴ On the other hand, for $T_p < T < T_M$ we find that the intensity of the Bragg peaks is weakly dependent on system size. The clear change of behavior of the size dependence gives a good criterion to determine T_M (Fig. 11).

The helicity modulus in the direction perpendicular to the current, Υ_x , decreases very slowly for $T < T_p$. Above T_p , Υ_x has a faster decay with important fluctuations and tends to vanish at T_M . For $T > T_M$, Υ_x oscillates around zero.

Therefore, for a small finite current the depinning and melting transitions become separated with $T_p < T_M$.

B. Intermediate currents

At intermediate currents, $0.04 < I < I_c(0)$, a *new* transition appears: the *transverse depinning* of the moving vortex lattice. As discussed in Sec.V, one can measure transverse depinning by applying a small transverse current while the VL is driven with a fixed longitudinal current. This is shown in Fig. 12(a) for the case of $I = 0.06$ and a small transverse current, $I_{tr} = 0.01$. We see that there is an onset of transverse voltage at $T_{tr} = 0.02$. We can also see that this transverse depinning temperature is above the depinning temperature T_p for longitudinal resistance [Fig.12(b), $T_p = 0.013$], and below the melting temperature T_M for the vanishing of the Bragg peaks [Fig.12(c), $T_M = 0.037$]. Therefore, this transition occurs at an intermediate temperature between the depinning and the melting transitions, $T_p < T_{tr} < T_M$. We also show in Fig.12(d) that the helicity modulus begins to fall down slowly at T_{tr} , while for $T_{tr} < T < T_M$ it has strong fluctuations, being difficult to interpret its behavior in this case.

It is interesting to study in more detail the behavior of the structure factor through all these transitions. The temperature dependence of the intensity of the Bragg peaks is shown in Fig.12(c). In Fig.13 we show examples of the structure factor $S(\mathbf{k})$ at temperatures in the different regimes. In the pinned phase, the $S(\mathbf{k})$ is nearly the same as in the ground state with delta-like Bragg peaks, see Fig.13(a). For the moving VL, we can see that there is less anisotropy in the *transversely pinned* regime $T_p < T < T_{tr}$ [Fig.13(b)] than in the *floating* regime $T_{tr} < T < T_M$ [Fig.13(c-d)]. Also in the inset of Fig.12(c) one can see that the intensity of the Bragg peaks has a greater dependence with size for $T_{tr} < T < T_M$ when compared with the $T_p < T < T_{tr}$ regime. Moreover, near T_M the VL structure becomes strongly anisotropic, with the peak at \mathbf{G}_1 much larger than the peak at \mathbf{G}_2 , see Fig.13(d).

The anisotropy of the Bragg peaks of the moving VL (in the regimes at $T_p < T < T_M$) has two characteristics: (i) the *width* of the peaks increases with T in the direction of the applied current (the direction perpendicular to the vortex motion), and (ii) the *height* of the peaks decreases in the direction of vortex motion. This can be observed in the sequence of structure factors shown in Fig.13(b-d). The details of the broadening of the Bragg peaks are shown in Fig.14(a) for the transversely pinned regime ($T_p < T = 0.018 < T_{tr}$) and in Fig.14(b) for the floating solid regime ($T_{tr} < T = 0.023 < T_M$).

In Fig.15 we show the temperature dependence of $S(\mathbf{G}_1)$ and $S(\mathbf{G}_2)$ for different currents. In all the cases the three different regimes in temperatures are observed: (i) pinned regime for $0 < T < T_p$ with isotropic and size independent Bragg peaks, (ii) transversely pinned regime for $T_p < T < T_{tr}$ with weakly anisotropic Bragg peaks, and (iii) the floating solid regime for $T_{tr} < T < T_M$ with strong anisotropy and size dependence in the Bragg

peaks.

C. High currents

In the case of currents larger than $I_c(0)$, the vortex lattice is already depinned at $T = 0$. As we have seen in Sec. V, this zero-temperature moving VL has a finite transverse critical current, and therefore it is pinned in the transverse direction. When we slowly increase temperature from this state, we find that the transverse resistive response is negligible for finite low temperatures. At a temperature T_{tr} there is a jump to a finite transverse resistance $R_{tr} = V_{tr}/I_{tr}$. For example, this is shown for $I = 0.16$ with a small transverse current, $I_x = 0.01$ in Fig.16(a). The vortex lattice has an anisotropic structural order for all temperatures, *i.e.*, $S(\mathbf{G}_1) \neq S(\mathbf{G}_2)$, and the height of the Bragg peaks vanishes at T_M , Fig.16(b). In the inset we show $S(\mathbf{G}_2)$ for different sizes, $L = 50, 100$, and we see that T_M is size independent. Similar behaviour is found for $S(\mathbf{G}_1)$. The transverse helicity modulus (Υ_x) is almost constant for low temperatures and starts to decrease at T_{tr} presenting strong fluctuations for $T > T_{tr}$, Fig16(c).

The analysis of the heights of the peaks in $S(\mathbf{k})$ as a function of system size L is a good indicator of the translational correlations in the system. This dependence is well known for two dimensional lattices.¹⁴ For a pinned solid $S(\mathbf{G}) \sim 1$, for a floating solid, $S(\mathbf{G}) \sim L^{-\eta_G(I,T)}$ with $0 < \eta_G(I,T) < 2$, being this dependence a signature of quasi-long range order, and for a normal liquid $S(\mathbf{G}) \sim L^{-2}$. To assure the existence of algebraic translational correlations, we have done this scaling study for currents $0.02 < I < 0.2$ and different temperatures for system sizes of $L = 50, 100, 150$. For the cases corresponding to the pinned regime ($T < T_p$) we found $\eta_G \approx 0$, as expected. In the transversely pinned regime, we show a case in Fig.17(a), we find a power law fitting with very small values of $\eta_G(I,T)$. In the floating regime, we find larger values of η_G , we show a case in Fig. 17(b). In all the cases we have obtained that $0 < \eta_G(I,T) < 2$ for $T_p < T < T_M$. Therefore, this finite size analysis shows the existence of quasi-long range order in the moving VL. Also, we find that $\eta_{G_1} > \eta_{G_2}$ for all currents and temperatures. The power-law exponent η_G can be studied at a constant current, as a function of temperature. This is shown in Fig.18, for $I = 0.16$ and different reciprocal lattice vectors. The exponent η is finite for the complete temperature range. For $T < T_{tr}$ it has a small value $\eta_G \approx 0.01$. It has a fast increase near T_{tr} , where there is also a clear difference between η_{G_1} and η_{G_2} . Finally, it reaches a value of $\eta = 2$ near $T = T_M$.

VII. ORIENTATIONAL PINNING EFFECTS

A very interesting characterization of the different regimes can be obtained by studying the effects of varying current direction.^{24,42,43} We apply a current I at an angle ϕ with respect to the [10] lattice direction,

$$\begin{aligned} I_x &= I \cos \phi \\ I_y &= I \sin \phi. \end{aligned} \quad (21)$$

We study the voltage response when varying the orientation ϕ of the drive while keeping fixed the amplitude I of the current. In the parametric curves of $V_y(\phi)$ vs. $V_x(\phi)$ can we analyze the breaking of rotational symmetry in the different regimes of I and T . In the case of rotational symmetry this kind of plot should give a perfect circle. However, the square symmetry of the Josephson lattice will show up in the shape of the curves. In Ref. 24 the motion of single vortices was studied. In this case, the ‘‘diagonal’’ [11] direction is unstable against small changes in the angle ϕ , while the [10] and [01] directions are the preferred directions for vortex motion.²⁴ This shows as ‘‘horns’’ in parametric V_y vs. V_x plots, which are finite segments of points lying in the x or the y axis. This implies the existence of transverse pinning in these directions (thus, it corresponds to orientational pinning). Here, we perform the same analysis for the different regimes of the moving VL.

In Fig.19 we plot the voltages V_y and V_x when varying the orientational angle ϕ for different current amplitudes I and temperatures T . In Fig.19(a) we have $I = 0.06$ and $T = 0.015$, corresponding to the regime of a transversely pinned lattice. In this case most of the points are lying either on the axis $V_x = 0$ or on the axis $V_y = 0$, indicating strong orientational pinning in the symmetry lattice directions [10] and [01]. When increasing T the orientational pinning decreases and the length of the ‘‘horns’’ in the x and y axis decreases. Fig.19(b) shows results for $I = 0.06$ and $T = 0.03$, which correspond to $T > T_{tr}$ when there is a finite transverse resistance. In this case the horns have disappeared and orientational pinning is lost. However, the breaking of rotational symmetry is still present in the star-shaped curves. Also in the high current regime, Fig.19(c), for a low temperature $T = 0.015$ ($T < T_{tr}$) we see that there is orientational pinning with the presence of horns, which again disappear for $T > T_{tr}$ as it is shown in Fig.19(d) at $T = 0.035$. Finally for $T \gg T_M$, deep inside in the liquid phase, the stars tend to the circular shape of rotational invariance.

VIII. DISCUSSION

With all the information of the previous sections we obtain the current-temperature phase diagram which was advanced in Fig.1. For finite currents we have been able to identify three different regimes, a *pinned VL* for $T <$

$T_p(I)$, a *transversely pinned VL* for $T_p(I) < T < T_{tr}(I)$, and a *floating VL* for $T_{tr}(I) < T < T_M(I)$. It is, however, difficult to define if the temperatures T_p, T_{tr}, T_M correspond to either phase transitions or to dynamical crossovers. The comparisons we have made of the behavior of voltages (longitudinal and transversal), structure factor and helicity modulus show that something is happening at these temperatures. Also, the comparison for different system sizes of the behavior of $S(\mathbf{G})$ suggest transitions for T_p, T_{tr}, T_M . The transverse helicity modulus has strong fluctuations for $T_{tr} < T < T_M$. These fluctuations are not reduced when increasing the simulation time in a factor of 10. This could mean that actually the range of temperatures of $T_{tr} < T < T_M$ corresponds to a long crossover region towards a liquid state. Also, one may question if the use of the helicity modulus for these far from equilibrium states is correct, since Υ_x has been defined from the response of the equilibrium free energy to a twist in the boundary condition. Most likely, the large fluctuations in $T_{tr} < T < T_M$ are due to the very unstable and history-dependent steady states we find in this regime. For example the steady states obtained when increasing temperature from $T = 0$ at fixed current differ from the steady states obtained when increasing current at fixed temperature in this regime. They differ in the degree of anisotropy and intensity of the Bragg peaks in the structure factor. We think that this reflects the fact that the VL is unpinned in all directions and the orientation of the moving state will depend on the history for this regime.

In any case, we can clearly distinguish different dynamical states which define the regimes shown in the phase diagram of Fig.1. From the experimental point of view these transitions (or crossovers) are possible to measure. The depinning temperature T_p can be obtained from resistance measurements at finite currents. The transverse current-voltage characteristics and the transverse resistivity can be measured for different longitudinal currents and temperatures, and therefore T_{tr} could be obtained. The helicity modulus can be measured with the two-coil technique.³ It could be very interesting to see the results of such measurements at finite currents. The structure factor and melting transition can not be measured directly. However, in the presence of an external rf current, the disappearance of Shapiro steps can indicate the melting transition,⁴⁷ since they are sensitive to the translational order of the vortex lattice.⁴⁸ Therefore, we expect that the results obtained here could motivate new experiments for fractional or submatching fields in Josephson junction arrays as well as in other superconductors with periodic pinning.

ACKNOWLEDGMENTS

We acknowledge fruitful discussions with H. Pastoriza and J. V. José. This work was supported by CONICET,

CNEA, ANPCyT (PICT Nro. 03-00121-02151) and Fundación Antorchas (Proyecto Nro. 13532/1-96).

APPENDIX A: PERIODIC BOUNDARY CONDITIONS

1. Phases

We want to obtain the periodic boundary condition (PBC) for superconducting phases $\theta(n_x, n_y)$. In general we can write the PBC as:

$$\begin{aligned}\theta(\mathbf{n} + \mathbf{L}_x) &= \theta(\mathbf{n}) + u_x(\mathbf{n}) \\ \theta(\mathbf{n} + \mathbf{L}_y) &= \theta(\mathbf{n}) + u_y(\mathbf{n}),\end{aligned}\quad (\text{A1})$$

where $\mathbf{L}_x = (L_x, 0)$ and $\mathbf{L}_y = (0, L_y)$. Taking into account that all variables should be independent of the order of subsequent global translations and that the phases are defined except for an addition of $2\pi l$, we are lead to the consistency condition

$$u_x(\mathbf{n}) + u_y(\mathbf{n} + \mathbf{L}_x) = u_x(\mathbf{n} + \mathbf{L}_y) + u_y(\mathbf{n}) + 2\pi l, \quad (\text{A2})$$

Therefore, in order to specify the periodic boundary conditions we have to give the functions u_x, u_y , which will depend on the gauge for the vector potential \mathbf{A} .

The periodic boundary condition for the phases can be deduced by requiring that all physical quantities are invariant after a translation in the lattice size. The supercurrents $S_\mu(\mathbf{n}) = \sin[\Delta_\mu\theta(\mathbf{n}) - A_\mu(\mathbf{n})]$ should satisfy:

$$\begin{aligned}S_\mu(\mathbf{n} + \mathbf{L}_x) &= S_\mu(\mathbf{n}) \\ S_\mu(\mathbf{n} + \mathbf{L}_y) &= S_\mu(\mathbf{n}).\end{aligned}\quad (\text{A3})$$

This implies that the gauge invariant phase difference $\theta_\mu(\mathbf{n}) = \Delta_\mu\theta(\mathbf{n}) - A_\mu(\mathbf{n})$ should satisfy

$$\begin{aligned}\theta_\mu(\mathbf{n} + \mathbf{L}_x) &= \theta_\mu(\mathbf{n}) + 2\pi l \\ \theta_\mu(\mathbf{n} + \mathbf{L}_y) &= \theta_\mu(\mathbf{n}) + 2\pi l',\end{aligned}\quad (\text{A4})$$

with l, l' any integer. This condition leads to

$$\begin{aligned}\Delta_\mu u_x(\mathbf{n}) &= 2\pi l + A_\mu(\mathbf{n} + \mathbf{L}_x) - A_\mu(\mathbf{n}) \\ \Delta_\mu u_y(\mathbf{n}) &= 2\pi l' + A_\mu(\mathbf{n} + \mathbf{L}_y) - A_\mu(\mathbf{n}).\end{aligned}\quad (\text{A5})$$

We can choose the solution with $l = l' = 0$. In the Landau gauge, A_x is a linear function of n_y and A_y is a linear function of n_x . Taking the origin such that $A_\mu(\mathbf{n} = 0) = 0$, we obtain for the Landau gauge:

$$\begin{aligned}u_x(\mathbf{n}) &= u_x(0) + A_y(\mathbf{L}_x)n_y \\ u_y(\mathbf{n}) &= u_y(0) + A_x(\mathbf{L}_y)n_x.\end{aligned}\quad (\text{A6})$$

The consistency condition (A2) requires

$$A_y(\mathbf{L}_x)L_y - A_x(\mathbf{L}_y)L_x = 2\pi l. \quad (\text{A7})$$

The term in the left side is equal to the total flux $2\pi f L_x L_y$, therefore (A7) is equivalent to flux quantization, giving $f L_x L_y = N_v$, with $N_v = l$ the number of vortices.

If we take $u_x(0) = u_y(0) = 0$, we obtain for the PBC

$$\begin{aligned}\theta(n_x + L_x, n_y) &= \theta(n_x, n_y) + A_y(\mathbf{L}_x) n_y \\ \theta(n_x, n_y + L_y) &= \theta(n_x, n_y) + A_x(\mathbf{L}_y) n_x.\end{aligned}\quad (\text{A8})$$

A particular choice can be the gauge with $A_x(\mathbf{n}) = -2\pi f n_y$, $A_y(\mathbf{n}) = 0$, which leads to Eq. (7).

2. External currents and electric fields

In the presence of external currents or voltages the periodic boundary conditions have to be reconsidered. In this case it is possible to have $\oint \mathbf{E} \cdot d\mathbf{l} \neq 0$ in a path that encloses all the sample either in the x or the y direction. Therefore, in a closed path we have to consider the Faraday's law

$$\oint \mathbf{E} \cdot d\mathbf{l} = -\frac{1}{c} \frac{d\Phi}{dt}.$$

The two-dimensional sample with PBC can be thought as the surface of a torus in three-dimensions. The closed paths we are considering are the two pathes that encircle the torus. The electric field is not a gradient of a potential, it is now given by $\mathbf{E} = -\nabla V - \frac{1}{c} \frac{\partial \mathbf{A}}{\partial t}$. One possible solution is to consider a vector potential

$$\mathbf{A}(\mathbf{r}, t) = \mathbf{A}_0(\mathbf{r}) - \vec{\alpha}(t),$$

for which

$$\begin{aligned}\mathbf{H}_{\text{ext}} &= \nabla \times \mathbf{A}_0 \\ \mathbf{E}_{\text{total}} &= \frac{1}{c} \frac{d\vec{\alpha}}{dt}\end{aligned}$$

In our case, we take the adimensional vector potential as:

$$A_\mu(\mathbf{n}, t) = A_\mu^0(\mathbf{n}) - \alpha_\mu(t), \quad (\text{A9})$$

with $A_\mu^0(\mathbf{n})$ in the Landau gauge ($A_x^0(\mathbf{n}) = -2\pi f n_y$, $A_y^0(\mathbf{n}) = 0$). Therefore the gauge invariant phase is:

$$\theta_\mu(\mathbf{n}, t) = \Delta_\mu \theta(\mathbf{n}, t) - A_\mu^0(\mathbf{n}) + \alpha_\mu(t).$$

Then α_μ acts as a global time-dependent phase in the μ direction.

In the normalized units used in this paper, the electric field in the link defined by the junction \mathbf{n}, μ is

$$E_\mu(\mathbf{n}) = -\Delta_\mu V(\mathbf{n}) - \frac{dA_\mu(\mathbf{n})}{dt},$$

where the electrostatic potential is $V(\mathbf{n}) = -\frac{d\theta(\mathbf{n})}{dt}$. Therefore we have

$$E_\mu(\mathbf{n}) = \Delta_\mu \frac{d\theta(\mathbf{n})}{dt} + \frac{d\alpha_\mu}{dt}.$$

The average electric field in the μ direction is:

$$E_\mu^{\text{av}} = \frac{1}{L_x L_y} \sum_{\mathbf{n}} E_\mu(\mathbf{n}) = \frac{d\alpha_\mu}{dt},$$

where we have used the fact that $\sum_{\mathbf{n}} \Delta_\mu \frac{d\theta(\mathbf{n})}{dt} = 0$ (which is the discrete equivalent of $\oint \nabla V \cdot d\mathbf{l} = 0$). The current in the link \mathbf{n}, μ is, in normalized units,:

$$I_\mu(\mathbf{n}) = E_\mu(\mathbf{n}) + \tilde{S}_\mu(\mathbf{n}),$$

with $\tilde{S}_\mu(\mathbf{n}) = S_\mu(\mathbf{n}) + \eta_\mu(\mathbf{n}, t)$. Therefore the average current in the μ direction is

$$I_\mu^{\text{av}} = \frac{1}{L_x L_y} \sum_{\mathbf{n}} I_\mu(\mathbf{n}) = E_\mu^{\text{av}} + S_\mu^{\text{av}} + \eta_\mu^{\text{av}} = \frac{d\alpha_\mu}{dt} + \frac{1}{L_x L_y} \sum_{\mathbf{n}} \tilde{S}_\mu(\mathbf{n})$$

There are two cases to consider: (i) *external current source*: the external current is given and the total voltage fluctuates and (ii) *external voltage source*: the external voltage is given and the total current fluctuates.

(i) *External current source*: the average current in μ direction is fixed by the external current: $I_\mu^{\text{av}} = I_\mu^{\text{ext}}$. The average electric field is a fluctuating quantity given by:

$$E_\mu^{\text{av}}(t) = \frac{d\alpha_\mu}{dt} = I_\mu^{\text{ext}} - \frac{1}{L_x L_y} \sum_{\mathbf{n}} \tilde{S}_\mu(\mathbf{n}). \quad (\text{A10})$$

In this case, the $\alpha_\mu(t)$ is a dynamical variable, and its time evolution is given by Eq.(A10).

(ii) *External voltage source*: the average electric field in the μ direction is fixed by the external electric field: $E_\mu^{\text{av}} = E_\mu^{\text{ext}}$. Therefore, now the α_μ is given by the external source:

$$\alpha_\mu(t) = \int E_\mu^{\text{ext}} dt,$$

and $\alpha_\mu(t) = E_\mu^{\text{ext}} t$, if E_μ^{ext} is time-independent. The average current is now a fluctuating quantity given by:

$$I_\mu^{\text{av}} = E_\mu^{\text{ext}} + \frac{1}{L_x L_y} \sum_{\mathbf{n}} \tilde{S}_\mu(\mathbf{n}).$$

Let us see how the PBC are affected by a change of gauge. The gauge transformations are the following:

$$\begin{aligned}\theta(\mathbf{n}) &\rightarrow \theta'(\mathbf{n}) = \theta(\mathbf{n}) + \phi(\mathbf{n}) \\ A_\mu(\mathbf{n}) &\rightarrow A'_\mu(\mathbf{n}) = A_\mu(\mathbf{n}) + \Delta_\mu \phi(\mathbf{n}) \\ V(\mathbf{n}) &\rightarrow V'(\mathbf{n}) = V(\mathbf{n}) - \frac{d\phi(\mathbf{n})}{dt}\end{aligned}$$

An interesting choice is:

$$\phi(\mathbf{n}) = \vec{\alpha} \cdot \mathbf{n} = \sum_{\mu} \alpha_\mu n_\mu$$

In this gauge we have $\theta_\mu(\mathbf{n}) = \Delta_\mu \theta(\mathbf{n}) - A_\mu^0(\mathbf{n})$ and the PBC for the phases is:

$$\begin{aligned}\theta(\mathbf{n} + \mathbf{L}_x) &= \theta(\mathbf{n}) + A_y(\mathbf{L}_x)n_y + \alpha_x L_x \\ \theta(\mathbf{n} + \mathbf{L}_y) &= \theta(\mathbf{n}) + A_x(\mathbf{L}_y)n_x + \alpha_y L_y,\end{aligned}\quad (\text{A11})$$

and for the voltages:

$$V(\mathbf{n} + \mathbf{L}_\mu) = V(\mathbf{n}) - \frac{d\alpha_\mu}{dt} L_\mu = V(\mathbf{n}) - E_\mu^{\text{av}} L_\mu \quad (\text{A12})$$

The equations of motion in this gauge are:

$$\begin{aligned}\frac{d\theta(\mathbf{n})}{dt} &= \sum_\mu \frac{d\alpha_\mu}{dt} n_\mu - \sum_{\mathbf{n}'} G_{\mathbf{n},\mathbf{n}'} \Delta_\mu \cdot \tilde{S}_\mu(\mathbf{n}') \\ \frac{d\alpha_\mu}{dt} &= I_\mu^{\text{ext}} - \frac{1}{L_x L_y} \sum_{\mathbf{n}} \tilde{S}_\mu(\mathbf{n})\end{aligned}\quad (\text{A13})$$

The periodic boundary conditions with a fixed external current using Eq. (A10) was used previously in Ref. 45 for $f = 0$ (it was called a ‘‘fluctuating twist boundary condition’’) and in Ref. 31 for $f \neq 0$. Also, the periodic boundary conditions in the gauge of Eqs. (A11-A12) were used in Ref. 44 for a time dependent d -wave Ginzburg-Landau model.

3. Helicity modulus

The helicity modulus Υ_μ expresses the ‘‘rigidity’’ of the system with respect to an applied ‘‘twist’’ in the periodic boundary conditions. The twist k_μ is defined as a phase change of $L_\mu k_\mu$ between the two opposite boundaries which are connected through the PBC in the μ direction

$$\theta(\mathbf{n} + \mathbf{L}_\mu) = \theta(\mathbf{n}) + L_\mu k_\mu.$$

The helicity modulus is obtained from the free energy $F(T, k_\mu)$ as:

$$\Upsilon_\mu = \frac{1}{L^2} \left. \frac{\partial^2 F(T, k_\mu)}{\partial k_\mu^2} \right|_{k_\mu=0} \quad (\text{A14})$$

It is clear from Eq. (A11) that $k_\mu = \alpha_\mu$. Then, in order to evaluate the helicity modulus, α_μ must be set to zero. This means that the helicity modulus can not be calculated in the direction in which there is an applied current, since it gives a fluctuating twist $k_\mu(t)$.

4. Algorithm

The core of the numerical calculation is to invert the Eq. (9). This means to solve a discrete Poisson equation of the form,

$$\Delta_\mu^2 f(\mathbf{n}) = d(\mathbf{n}) \quad (\text{A15})$$

with the periodic boundary conditions

$$\begin{aligned}f(\mathbf{n} + \mathbf{L}_x) &= f(\mathbf{n}) \\ f(\mathbf{n} + \mathbf{L}_y) &= f(\mathbf{n}).\end{aligned}\quad (\text{A16})$$

The linear system of $L_x L_y$ equations of (A15) is singular. Physically, the reason is that in Eq.(9), $f(\mathbf{n}) = d\theta(\mathbf{n})/dt$ corresponds to a voltage, which is defined except for a constant. We choose the voltage reference such that it has zero mean:

$$\sum_{\mathbf{n}} f(\mathbf{n}) = 0, \quad (\text{A17})$$

other choices are also possible (like, for example, fixing $f(\mathbf{n}_0) = 0$ at a given site \mathbf{n}_0).

The method we use to invert the Eq. (A15) is based on the Fourier Accelerated and Cyclic Reduction (FACR) algorithm.⁴⁶ In this case, we take first the discrete Fourier transform in the x direction:

$$\tilde{d}(k_x, n_y) = \sum_{n_x} d(n_x, n_y) e^{i \frac{2\pi k_x n_x}{L_x}}, \quad (\text{A18})$$

which with a fast Fourier algorithm takes a computation time of order $L_x \log L_x$. This leads to the following equation:

$$\epsilon_{k_x} \tilde{f}(k_x, n_y) - \tilde{f}(k_x, n_y - 1) - \tilde{f}(k_x, n_y + 1) = \tilde{d}(k_x, n_y), \quad (\text{A19})$$

with $\epsilon_{k_x} = 4 - 2 \cos \frac{2\pi k_x}{L_x}$ and with boundary condition $\tilde{f}(k_x, L_y + 1) = \tilde{f}(k_x, 1)$. This is a cyclic tridiagonal equation which can be solved with a simple LU decomposition algorithm in a computation time of order L_y .⁴⁶ In this way the $\tilde{f}(k_x, n_y)$ is obtained from (A19). Finally we take the inverse Fourier transform to obtain

$$f(n_x, n_y) = \frac{1}{L_x} \sum_{k_x} \tilde{f}(k_x, n_y) e^{-i \frac{2\pi k_x n_x}{L_x}}. \quad (\text{A20})$$

This algorithm takes a computation time which is of order $L_x L_y (\log L_x + A)$ with the constant $A \sim 1$. This is faster than the two dimensional Fourier transform method used by Eikmans and van Himbergen,³⁴ which takes a computation time of order $L_x L_y (\log L_x + \log L_y)$.

¹ P. Martinoli, O. Daldini, C. Leemann, and E. Stocker, Solid State Comm. **17**, 205 (1975); P. Martinoli, O. Daldini, C. Leemann, and B. Van den Brandt, Phys. Rev. Lett. **36**, 382 (1976).

² B. Pannetier, J. Chaussy, R. Rammal, and J. C. Villegier, Phys. Rev. Lett. **53**, 1845 (1984); H. D. Hallen *et al.*, Phys. Rev. Lett. **71**, 3007 (1993); K. Runge and B. Pannetier, Europhys. Lett. **24**, 737 (1993).

- ³ For recent reviews in Josephson arrays see R. S. Newrock, C. J. Lobb, U. Geigenmuller and M. Octavio, *Solid State Physics* **54**, 263 (2000); *Lectures on superconducting networks and mesoscopic systems*, Ed. C. Giovanella and C. J. Lambert (American Institute of Physics, AIP Conf. Proc. 427, New York, 1998) See also J. C. Ciria and C. Giovanella, *J. Phys. Condes. Matter* **10**, 1453 (1998); *Macroscopic Quantum Phenomena and Coherence in Superconducting Networks*, Ed. C. Giovanella and M. Tinkham (World Scientific, Singapore, 1995) and *Proceedings of the ICTP Workshop on Josephson-junction arrays*, *Physica B* **222**, 253 (1996).
- ⁴ C. J. Lobb, D. W. Abraham. and M. Tinkham, *Phys. Rev. B* **27**, 150 (1983).
- ⁵ See for example M. S. Rzchowski, S. P. Benz, M. Tinkham, and C. J. Lobb, *Phys. Rev. B* **42**, 2041 (1990).
- ⁶ J. I. Martín, M. Vélez, J. Nogués, and Ivan K. Schuller, *Phys. Rev. Lett.* **79**, 1929 (1997); D. J. Morgan and J. B. Ketterson, *Phys. Rev. Lett.* **80**, 3614 (1998); Y. Jaccard *et al.*, *Phys. Rev. B* **58**, 8232 (1998); M.J. Van Bael *et al.*, *Phys. Rev. B* **59**, 14674 (1999); J.I.Martín *et al.*, *Phys. Rev. Lett.* **83**, 1022 (1999); T. Puig *et al.*, *Phys. Rev. B* **58**, 5744 (1998).
- ⁷ M. Baert, V. V. Metlushko, R. Jonckheere, V. V. Moshchalkov, and Y. Bruynseraede, *Phys. Rev. Lett* **74**, 3269 (1995); K. Harada, O. Kamimura, H. Kasai, T. Matsuda, A. Tonomura and V. V. Moshchalkov, *Science* **271**, 1393 (1996); J.Y. Lin *et al.*, *Phys. Rev. B* **54**, R12714 (1996); A. Bezryadin, Yu. B. Ovchinnikov, and B. Pannetier, *Phys. Rev. B* **53**, 8553 (1996); E. Rossel *et al.*, *Phys. Rev. B* **53**, R2983; A. Castellanos, R. Wondenweber, G. Ockenfuss, A. v.d. Hart, and K. Keck, *Appl. Phys. Lett.* **71**, 962 (1997) V. V. Moshchalkov, M. Baert, V. V. Metlushko, E. Rosseel, M. J. van Bael, K. Temst, Y Bruynseraede, and R. Jonckheere, *Phys. Rev. B* **57**, 3615 (1998); V. Metlushko *et al.*, *Phys. Rev. B* **59**, 603 (1999); V. Metlushko *et al.*, *Phys. Rev. B* **60**, 12585 (1999); L. V. Look *et al.*, *Phys. Rev. B* **60**, R6998 (1999).
- ⁸ S. B. Field, S. S. James, J. Barentine, V. Metlushko, G. Crabtree, H. Shtrikman, B. Ilic, and S. R. J. Brueck, preprint cond-mat/003415.
- ⁹ Y. Fasano, J. A. Herbsommer, F. de la Cruz, F. Pardo, P. L. Gammel, E. Bucher and D. J. Bishop, *Phys. Rev. B* **60**, R15047 (1999).
- ¹⁰ P. Martinoli, *Phys. Rev. B* **17**, 1175 (1978).
- ¹¹ V. L. Pokrovskii and A. L. Talanov, *Sov. Phys. JETTP* **51**, 134 (1980).
- ¹² P. Martinoli, M. Nsabimana, G. A. Racine and H. Beck, *Hel. Phys. Acta* **55**, 655 (1982).
- ¹³ D. R. Nelson in *Phase Transitions and Critical Phenomena*, edited by C. Domb and J. L. Lebowitz (Academic, New York, 1983), Vol. 7.
- ¹⁴ M. Franz and S. Teitel, *Phys. Rev. Lett.* **73**, 480 (1994) and *Phys. Rev. B* **51**, 6551 (1995).
- ¹⁵ S. Hattel and J. M. Wheatley, *Phys. Rev. B* **51**, 11951 (1995).
- ¹⁶ C. Reichhardt, C. J. Olson and F. Nori, *Phys. Rev. B* **54**, 16108 (1996); *Phys. Rev. B* **57**, 7937 (1998).
- ¹⁷ W. A. M. Morgado and G. Carneiro, *Physica C* **238**, 195 (1998).
- ¹⁸ C. Reichhardt, C. J. Olson and F. Nori, *Phys. Rev. Lett.* **78**, 2648 (1997); *Phys. Rev. B* **58**, 6534 (1998).
- ¹⁹ C. Reichhardt and F. Nori, *Phys. Rev. Lett.* **82**, 414 (1999).
- ²⁰ V. I. Marconi and D. Domínguez, *Phys. Rev. Lett* **82**, 4922 (1999).
- ²¹ G. Carneiro, *J. Low Temp. Phys.* **177**, 1323 (1999).
- ²² C. Reichhardt, G. Zimanyi, *Phys. Rev. B* **61**, 14354 (2000).
- ²³ G. Carneiro, preprint.
- ²⁴ V. I. Marconi, S. Candia, P. Balenzuela, H. Pastoriza, D. Domínguez and P. Martinoli, *Phys. Rev. B* (01 August 2000).
- ²⁵ A. E. Koshelev and V. M. Vinokur, *Phys. Rev. Lett.* **73**, 3580 (1994); S. Scheidl and V. M. Vinokur, *Phys. Rev. B* **57**, 13800 (1998).
- ²⁶ T. Giamarchi and P. Le Doussal, *Phys. Rev. Lett.* **76**, 3408 (1996); P. Le Doussal and T. Giamarchi, *Phys. Rev. B* **57**, 11356 (1998).
- ²⁷ L. Balents, M. C. Marchetti and L. Radzihovsky, *Phys. Rev. B* **57**, 7705 (1998).
- ²⁸ F. Pardo *et al.*, *Phys. Rev. Lett.* **78**, 4633 (1997); and *Nature* **396**, 398 (1998).
- ²⁹ K. Moon *et al.*, *Phys. Rev. Lett.* **77**, 2778 (1996); S. Ryu *et al.*, *Phys. Rev. Lett.* **77**, 5114 (1996); S. Spencer and H. J. Jensen, *Phys. Rev. B* **55**, 8473 (1997); C. J. Olson *et al.*, *Phys. Rev. Lett.* **81**, 3757 (1998); A. B. Kolton, D. Domínguez, N. Gronbech-Jensen, *Phys. Rev. Lett.* **83**, 3061 (1999); A. B. Kolton *et al.*, cond-mat/0004059.
- ³⁰ D. Domínguez, N. Grønbech-Jensen and A.R. Bishop, *Phys. Rev. Lett.* **78**, 2644 (1997).
- ³¹ D. Domínguez, *Phys. Rev. Lett.* **82**, 181 (1999).
- ³² J. S. Chung, K. H. Lee, and D. Stroud, *Phys. Rev. B* **40**, 6570 (1989), K. K. Mon and S. Teitel, *Phys. Rev. Lett.* **63**, 673 (1989).
- ³³ F. Faló, A. R. Bishop, and S. P. Lomdahl, *Phys. Rev. B* **41**, 10983 (1990).
- ³⁴ H. Eikmans and J.E. van Himbergen, *Phys. Rev. B* **41**, 8927 (1990).
- ³⁵ D. Domínguez, J. V. José, A. Karma and C. Wiecko, *Phys. Rev. Lett.* (1991) **67**, 2367; D. Domínguez, *Phys. Rev. Lett.* **72**, 3096 (1994).
- ³⁶ S. Kim and M. Y. Choi, *Phys. Rev. B* **48**, 322 (1993).
- ³⁷ W. Yu, K. H. Lee, and D. Stroud, *Phys. Rev. B* **47**, 5906 (1993).
- ³⁸ T. J. Hagenaars, P.H.E. Tiesinga, J.E. van Himbergen and J.V. José, *Phys. Rev. B* **50**, 1143 (1994).
- ³⁹ D. Domínguez and J. V. José, *Phys. Rev. B.* **53**, 11692 (1996).
- ⁴⁰ Y. H. Li and S. Teitel, *Phys. Rev. B* **47**, 359 (1993).
- ⁴¹ M. C. Hellerqvist *et al.*, *Phys. Rev. Lett.* **76**, 4022 (1996).
- ⁴² K. D. Fisher, D. Stroud and L. Janin, preprint cond-mat/9906068.
- ⁴³ M. Yoon, M. Y. Choi and B. J. Kim, *Phys. Rev. B* **61**, 3263 (2000).
- ⁴⁴ J. J. Vicente Alvarez, D. Domínguez and C. A. Balseiro, *Phys. Rev. Lett.* **79**, 1373 (1997).
- ⁴⁵ B. J. Kim, P. Minnhagen, and P. Olsson, *Phys. Rev. B* **59**, 11506 (1999).
- ⁴⁶ W. H. Press, S. A. Teukolsky, W. T. Vetterling and B. P. Flannery, *Numerical Recipes* (Cambridge University Press, New York, 1992).

⁴⁷ Harris *et al.*, Phys. Rev. Lett. (1995).

⁴⁸ V. I. Marconi and D. Domínguez, unpublished.

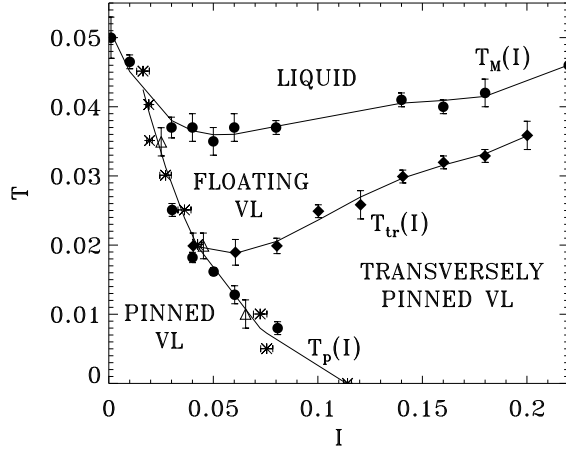


FIG. 1. $I - T$ Phase diagram for $f = 1/25$. $T_M(I)$ line is obtained from $S(\mathbf{G})$ vs. T curves (\bullet). $T_p(I)$ line is obtained from IV curves (\star), from $S(\mathbf{G})$ vs. T curves (\bullet) and from $\langle V_y \rangle$ vs. T curves (Δ). $T_{tr}(I)$ curve is obtained from $\langle V_{tr} \rangle$ vs. T curves (\blacklozenge).

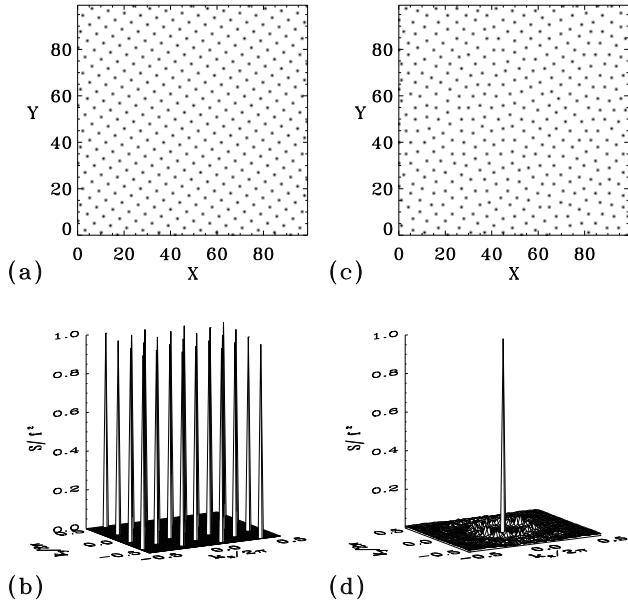


FIG. 2. Vortex configuration for a low current $I = 0.01 \ll I_c(0)$ and a low temperature, $T = 0.01 < T_M$: (a) tilted square vortex lattice, oriented in the $[4a, 3a]$ direction and (b) corresponding structure factor $S(\mathbf{k})$. At high temperature, $T = 0.05 \gtrsim T_M$: (c) disordered vortex array, (d) vortex liquid-like structure factor.

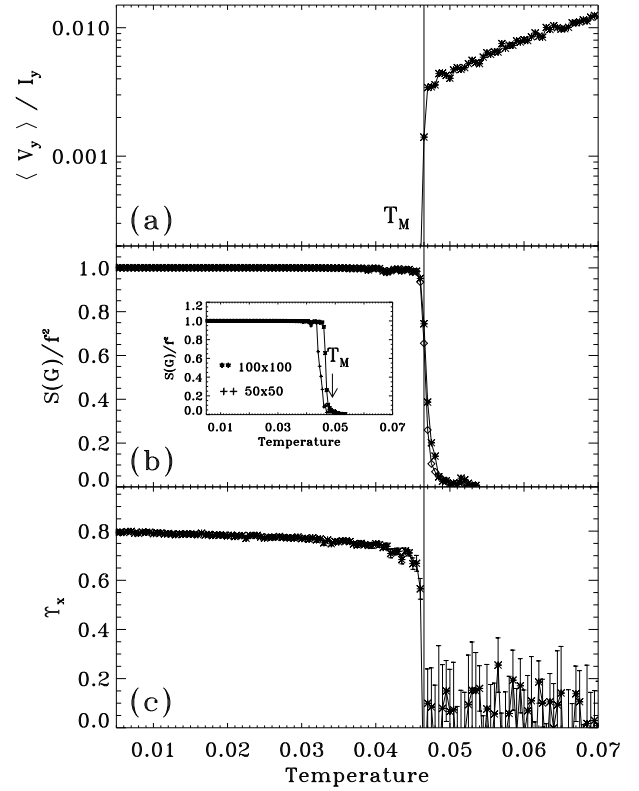


FIG. 3. For low current $I \ll I_c(0)$, $I = 0.01$: (a) $\langle V_y \rangle / I_y$ vs. T , (b) $S(\mathbf{G}_1)$ (\diamond) and $S(\mathbf{G}_2)$ (\star) vs. T , inset: size effect in $S(\mathbf{G}_1)$, (c) γ_x vs. T .

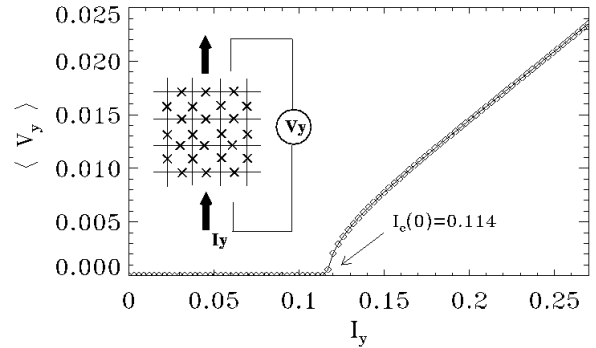


FIG. 4. Zero temperature IV curve. There is a critical current $I_c(0) = 0.114 \pm 0.002$.

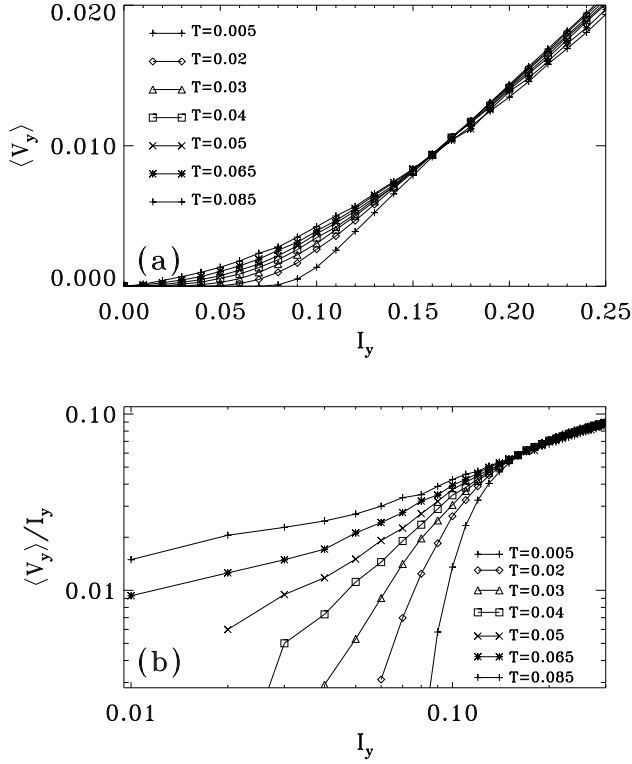


FIG. 5. IV curves for different temperatures. (a) Linear scale, crossing point at $I^* = 0.165$. (b) Log-log plot of $R = V/I$ vs. I for the same temperatures.

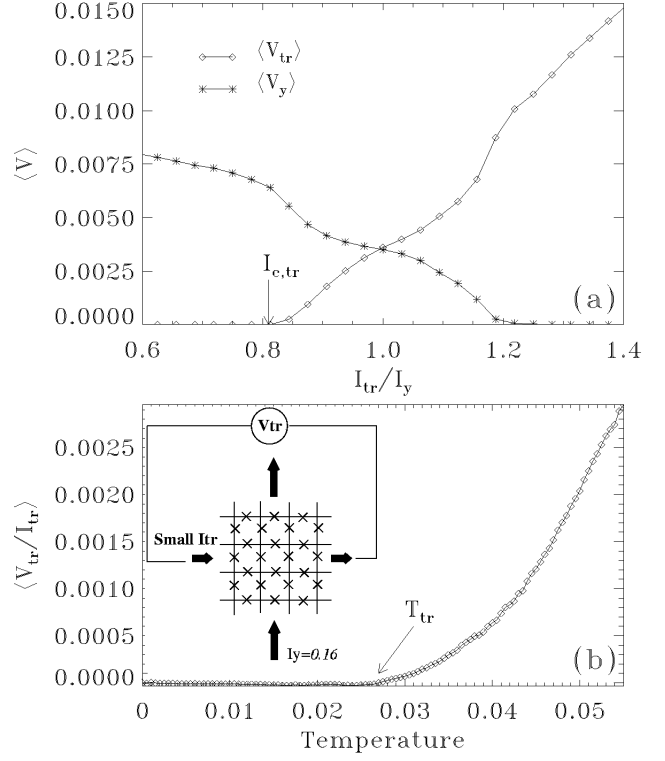


FIG. 7. Transverse depinning temperature determinations: (a) $Tr - IV$ curve and $\langle V_y \rangle$ vs I_{tr}/I_y at $T = 0$ and high longitudinal current, $I_y = 0.16$. (b) With small transverse current applied, $I_x = 0.01$, and $I_y = 0.16$, $\langle V_{tr}/I_{tr} \rangle$ vs T .

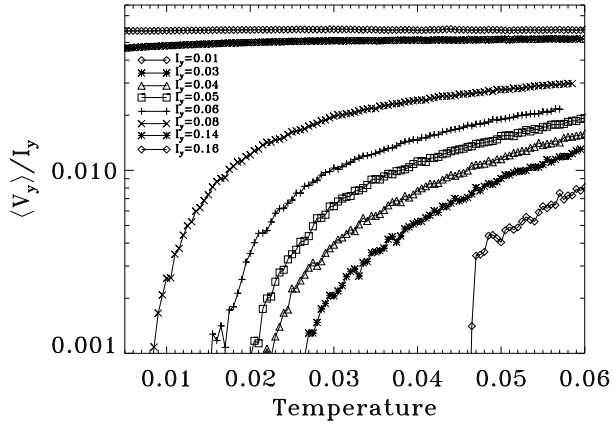


FIG. 6. $\langle V_y \rangle / I_y$ vs temperature curves for different dc currents (I_y).

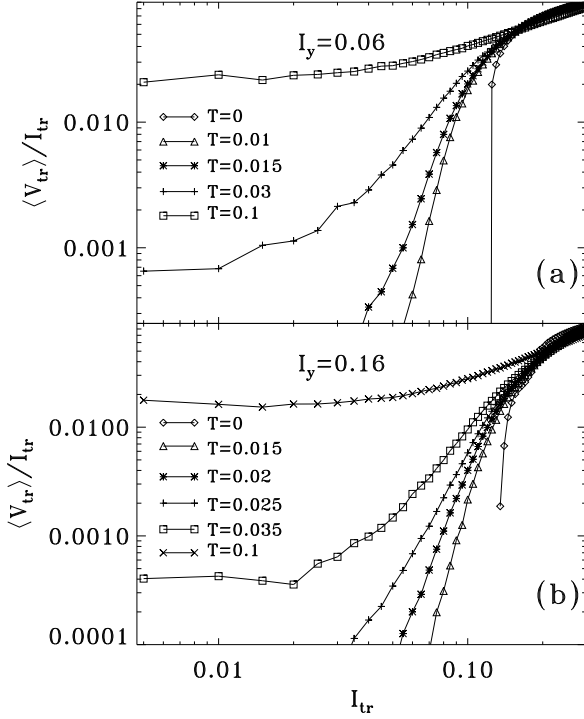


FIG. 8. Transverse IV curves for different temperatures: (a) low current $I_y < I_c(0)$, $I_y = 0.06$, (b) high current $I_y > I_c(0)$, $I_y = 0.16$.

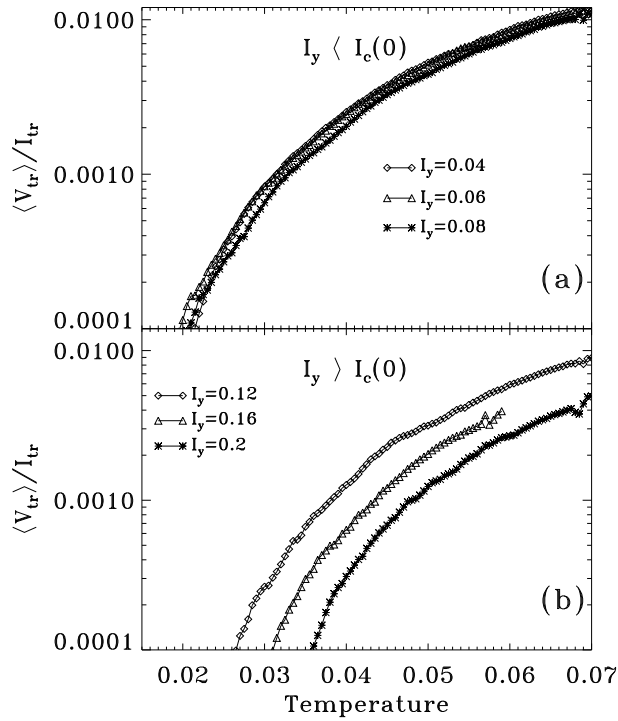


FIG. 9. V_{tr}/I_{tr} vs T curves for different dc currents applied in the y direction and small transverse current applied, $I_x = 0.01$: (a) low current $I_y < I_c(0)$, (b) high current $I_y > I_c(0)$.

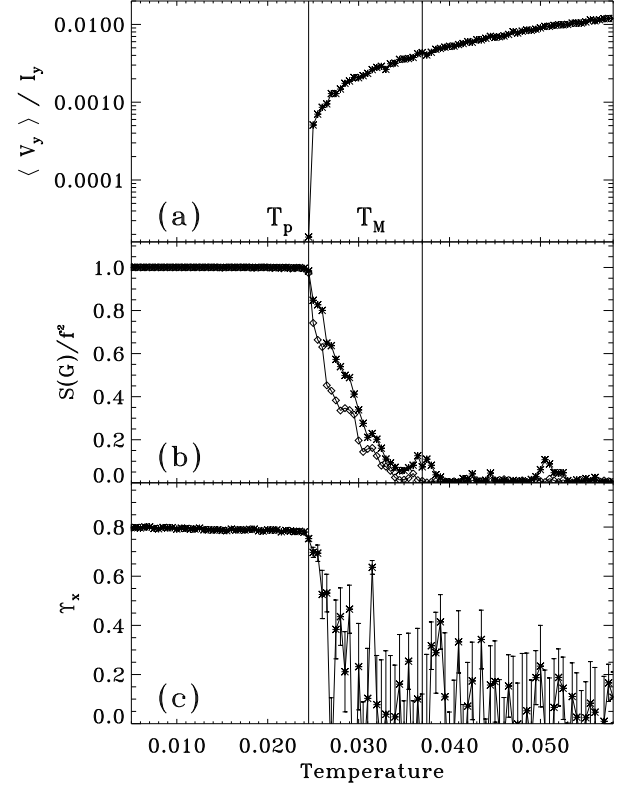


FIG. 10. For low current $I < I_c(0)$, $I = 0.03$: (a) $\langle V_y \rangle / I_y$ vs. T , (b) $S(G_1)$ (\diamond) and $S(G_2)$ (\star) vs. T , (c) Υ_x vs. T .

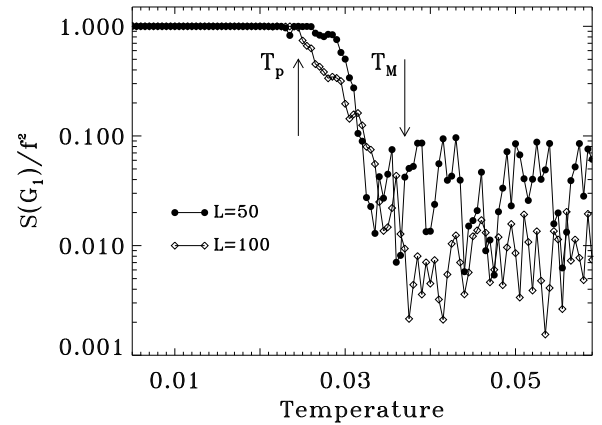


FIG. 11. For low current $I < I_c(0)$, $I = 0.03$: size effect in $S(G_1)$.

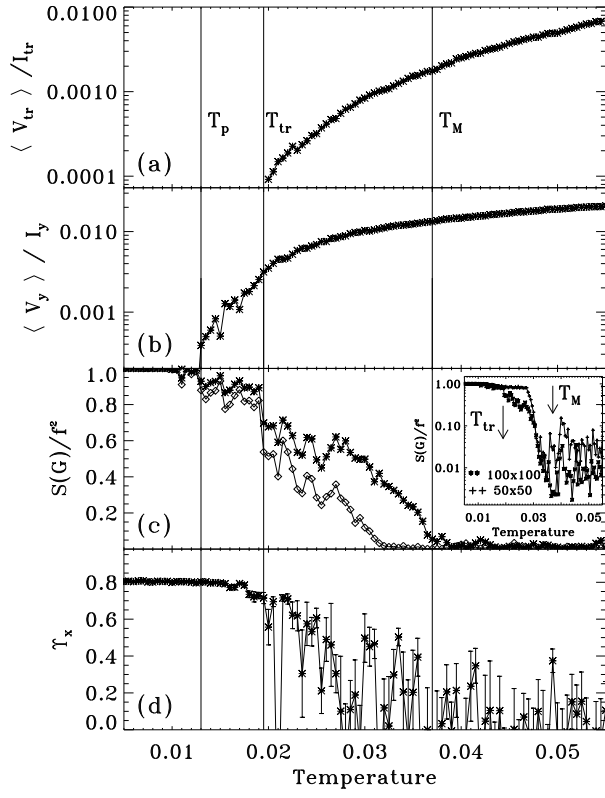


FIG. 12. For $I < I_c(0)$, $I = 0.06$: (a) $\langle V_{tr} \rangle / I_{tr}$ vs. T , (b) $\langle V_y \rangle / I_y$ vs. T , (c) $S(\mathbf{G}_1)$ (\diamond) and $S(\mathbf{G}_2)$ (\star) vs. T , inset: size effect in $S(\mathbf{G}_1)$, (d) γ_x vs. T .

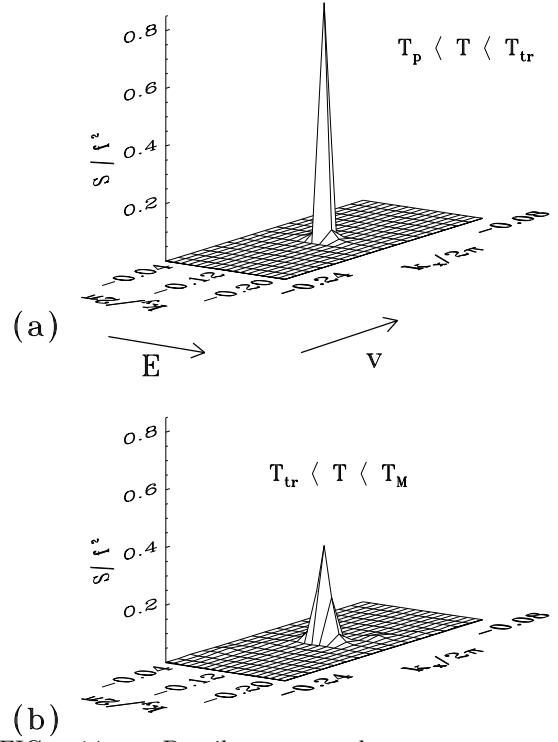


FIG. 14. Details on the structure factor peak, $\mathbf{G}_1 = \frac{2\pi}{a}(-4/25, -3/25)$, at $I < I_c(0)$, $I = 0.06$, for different temperatures: (a) $T_p < T < T_{tr}$, $T = 0.018$, (b) $T_{tr} < T < T_M$, $T = 0.023$.

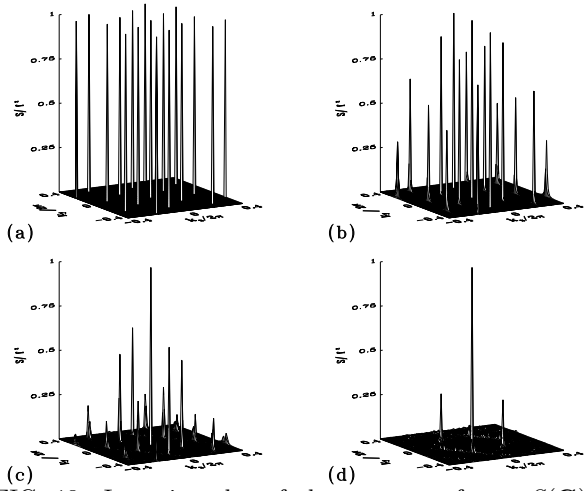


FIG. 13. Intensity plot of the structure factor $S(\mathbf{G})$ at $I < I_c(0)$, $I = 0.06$ for different temperatures: (a) $T < T_p$, $T = 0.0005$, (b) $T_p < T < T_{tr}$, $T = 0.015$, (c) $T_{tr} < T < T_M$, $T = 0.025$, (d) $T \leq T_M$, $T = 0.034$.

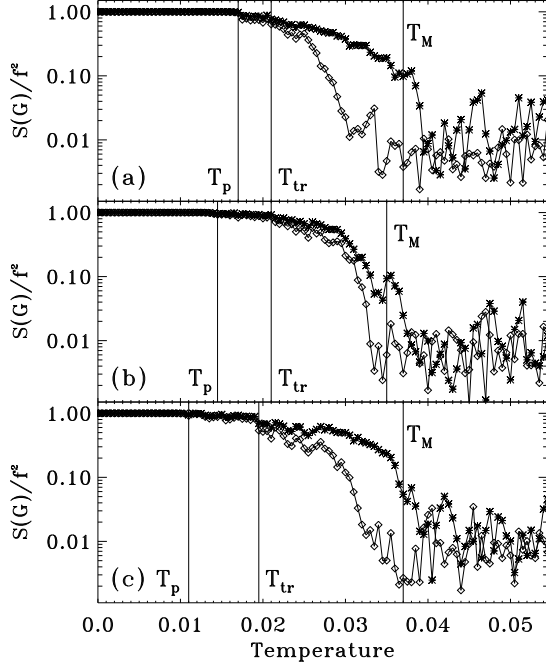


FIG. 15. $S(\mathbf{G}_1)$ (\diamond) and $S(\mathbf{G}_2)$ (\star) vs. T for different dc current applied in y direction: (a) $I_y = 0.04$, (b) $I_y = 0.05$, (c) $I_y = 0.06$.

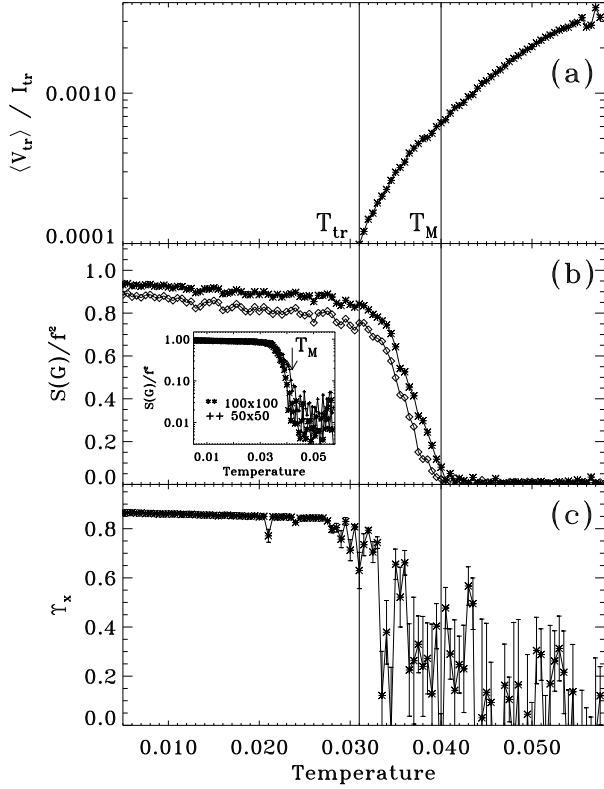


FIG. 16. For high current $I > I_c(0)$, $I = 0.16$: (a) $\langle V_{tr} \rangle / I_{tr}$ vs. T , (b) $S(\mathbf{G}_1)$ (\diamond) and $S(\mathbf{G}_2)$ (\star) vs. T , inset: size effect in $S(\mathbf{G}_2)$, (c) T_x vs. T .

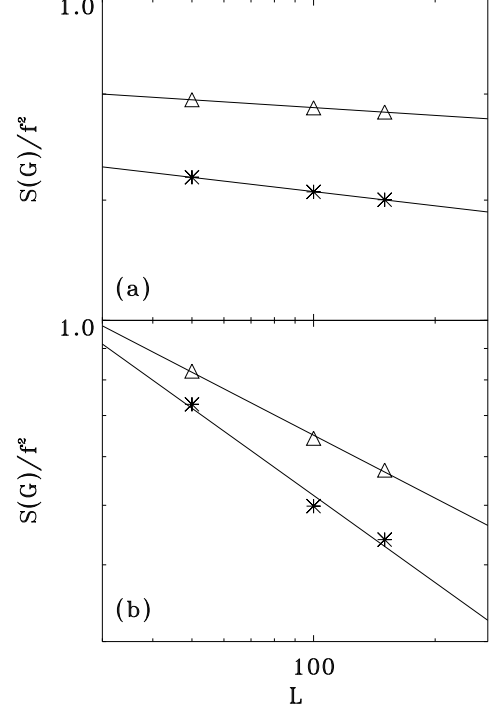


FIG. 17. Finite size analysis and power law fit of $S(\mathbf{G}) \sim L^{-\eta_{\mathbf{G}}}(I, T)$ for a moving vortex lattice at $I > I_c(0)$, $I = 0.16$. We obtain: (a) for $T < T_{tr}$, $T = 0.02$, $\eta_{G_1} = 0.023$ (\star) and $\eta_{G_2} = 0.013$, (Δ), (b) for $T_{tr} < T < T_M$, $T = 0.035$, $\eta_{G_1} = 0.471$ (\star) and $\eta_{G_2} = 0.34$ (Δ).

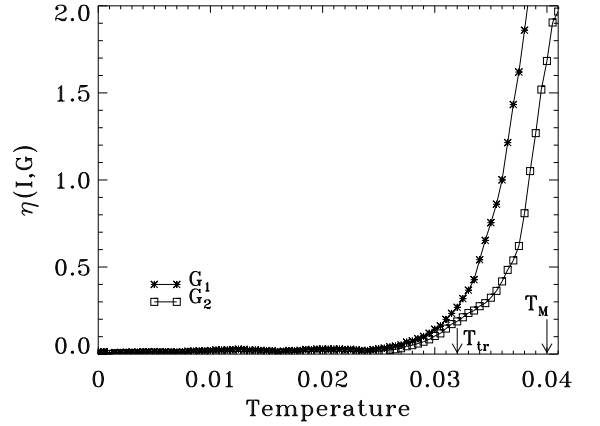


FIG. 18. At $I = 0.16$, $\eta(I, \mathbf{G})$ vs T , for \mathbf{G}_1 and \mathbf{G}_2 .

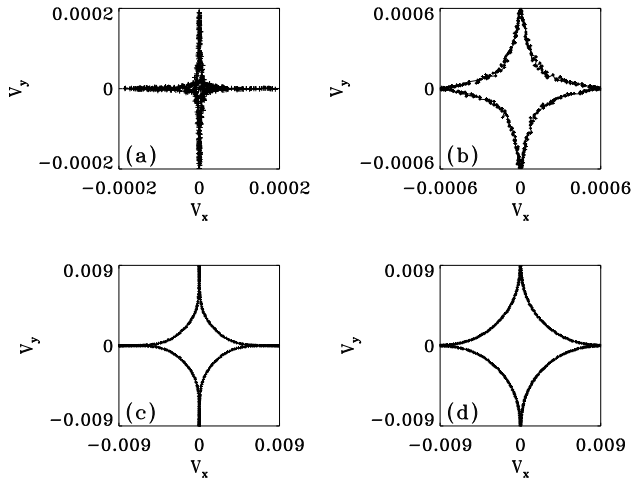


FIG. 19. Parametric curves $V_y(\phi)$ vs. $V_x(\phi)$ for different dc current applied and temperatures: (a) $|I_y| = 0.06$ and $T = 0.015$, (b) $|I_y| = 0.06$ and $T = 0.03$, (c) $|I_y| = 0.16$ and $T = 0.015$, (d) $|I_y| = 0.16$ and $T = 0.035$.